Fuel Cells

Fuel Cells
FROM FUNDAMENTALS TO SYSTEMS

SPECIAL ISSUE 10th-IHTECH

RESEARCH ARTICLE

Design of Thermal Management System Based on Phase Change Material for Fuel Cell Hybrid Electric Vehicles: A Numerical Study

Damla Yağci[1,2] | Hadi Genceli[2] | Oğuz Emrah Turgut[3]

[1]İstanbul Gelişim University, Department of Hybrid and Electric Vehicle Technologies, Istanbul, Türkiye | [2]Yildiz Technical University, Department of Mechanical Engineering, Istanbul, Türkiye | [3]İzmir Bakırçay University, Department of Industrial Engineering, İzmir, Türkiye

Correspondence: Damla Yağci (dyagci@gelisim.edu.tr) | Oğuz Emrah Turgut (oguzemrah.turgut@bakircay.edu.tr)

Received: 15 June 2026 | **Revised:** 20 July 2026 | **Accepted:** 27 July 2026

Guest Editor: Esmail Doustkhah

Keywords: fuel cell hybrid electric vehicles | PEM fuel cell | phase change material (PCM) | thermal energy storage | thermal management | waste heat recovery

ABSTRACT

In this study, a numerical analysis of the thermal management system for a fuel cell hybrid electric vehicle (FCHEV), based on the second-generation Toyota Mirai, has been conducted. Within the scope of the model, the fuel cell stack, electric motor, high-voltage battery, cabin heating/cooling system, and phase-change material (PCM) based thermal storage unit have been considered as a single integrated system. Hydrogen consumption, component temperatures, battery state of charge, the effect of regenerative braking, cabin thermal behavior, and waste heat recovery have been analyzed for summer and winter operating conditions within the WLTC Class 3 driving cycle. In the proposed model, while the fuel cell is regarded as the primary energy source, the battery functions as a secondary energy storage system, used to meet sudden power demands and to store energy recovered from regenerative braking. The control strategy is designed to recover waste heat energy generated by the fuel cell and electric motor for cabin heating and PCM charging. The model also considers dynamic battery SOC behavior, fuel-cell load-following operation, cabin thermal behavior, and PCM charge/discharge behavior. The results obtained demonstrate that the proposed integrated thermal management approach can utilize fuel cell and electric motor waste heat to support cabin heating, particularly in winter conditions. The simulated hydrogen consumption is 0.944 kg/100 km under WLTP-like conditions, within 6% of the certified value of 0.89 kg/100 km, rising to 0.989 and 1.007 kg/100 km under summer and winter HVAC loads, respectively. In winter, 29.2% of the powertrain waste heat is recovered; the pre-charged PCM unit delivers 1204 Wh of cabin heat, covers 73.9% of the delivered heating during the first 10 min of the cold start, and reduces the PTC consumption by 58.4% and the hydrogen consumption by 5.8% compared with the no-PCM baseline In conclusion, the PCM-assisted integrated thermal management system offers a measurable improvement in energy efficiency and cabin heating performance in fuel cell vehicles, but its effectiveness depends strongly on the control strategy, the initial thermal state of the storage, and the sizing of the PCM unit.

Abbreviations: ACS, air conditioning system; BTMS, battery thermal management system; EVs, electric vehicles; FCEVs, fuel cell electric vehicles; FCTMS, fuel cell thermal management system; MTMS, motor thermal management system; PCM, phase-change material; PEMFCs, proton exchange membrane fuel cells; PEVs, pure electric vehicles; PTC, positive temperature coefficient; TMS, thermal management system; VTMS, vehicle thermal management system; WLTC, Worldwide Harmonized Light Vehicle Test Cycle.

1 | Introduction

The long-term dependence on fossil fuels, particularly in the transportation sector, has become less favorable due to price volatility and environmental concerns. This situation has accelerated the shift toward cleaner and more efficient energy technologies. In recent years, the shift towards electric vehicles (EVs) has accelerated primarily to ensure energy supply security as well as decrease environmental pollution [1]. Despite these advances, limited driving range and long charging times remain essential challenges for battery-based pure electric vehicles (PEVs). These limitations have encouraged the development of alternative vehicle architectures. As a result, both researchers and automotive manufacturers have increasingly focused on hybrid electric vehicles (HEVs), which combine a battery with an internal combustion engine or a fuel cell [2, 3]. Fuel cell electric vehicles (FCEVs) contribute to decarbonizing the transportation sector because they have no direct CO_2 emissions during operation. In the coming years, fuel cell vehicles are anticipated to play an important role in transportation owing to their high efficiency and lower contribution to air pollution, with their acceptance having risen in recent years [4, 5]. In this context, PEMFCs have been widely considered as possible power sources for vehicles because of their relatively higher efficiency as well as the absence of CO_2 emissions. However, temperature significantly affects both the performance and lifetime of PEMFCs under various operating conditions. The temperature of a PEMFC is a determining factor influencing the rate of electrochemical reactions, transport phenomena, and water management inside the cell. Therefore, it becomes crucial to keep the PEMFCs within their ideal temperature range, which is necessary for fuel-cell-powered cars to function. The ideal temperature range for PEMFCs is between 60°C and 80°C, and the temperature differential between the stacks cannot be greater than 10°C, as reported by Tsushima et al. [6]. Operating fuel cells in the temperature intervals outside this interval may result in considerable reductions in performance, accelerated degradation, decreased durability, and shorter fuel cell life [7]. A thermal management system (TMS) is therefore critical in ensuring the effective and efficient performance of fuel cell vehicles that use PEMFC technology. For this reason, there have been several studies carried out on TMSs and their respective benefits and drawbacks. The VTMS in FCEVs is a sophisticated system. It includes the battery thermal management system (BTMS), motor thermal management system (MTMS), fuel cell thermal management system (FCTMS), and air conditioning system (ACS). The former three systems are very important in providing the necessary energy and power for the fuel cell vehicles to perform effectively in a safe environment [8].

Lithium-ion batteries offer high specific energy, low maintenance costs, and a low self-discharge rate. However, safety issues relating to leakage, high temperatures, and the formation of crystalline structures between the electrodes are significant concerns for lithium-ion batteries; therefore, appropriate thermal management is essential [9, 10]. Consequently, adequate cooling is essential to maintain the cell temperature within the operating range, making BTMS a critical component of high-power batteries used in electric or hybrid vehicles. In challenging environments, a large proportion of the energy is consumed by the TMS, making it difficult to maintain cell temperatures within a specific range. A review of the literature reveals numerous studies on the use of phase-change materials (PCMs) integrated into BTMS to address such issues [11]; furthermore, countless studies confirm the continuous growth and development of new-generation lithium-ion batteries [12, 13]. PCMs are widely used in thermal management applications, such as in the building industry [14] and in refrigeration systems, owing to their ability to store and release latent heat during the solid–liquid transition, thereby improving energy efficiency and reducing operating expenses. In the automotive field, the integration of PCMs has likewise been proven to be one of the most promising ways to overcome the thermal challenges of battery systems. In cold climates, thermal demands such as cabin heating impose an additional load on the battery and cause a considerable loss of driving range. PCM-based thermal batteries also offer an innovative solution to this challenge, thanks to their high energy storage capacity and phase-change mechanisms. Such systems store surplus energy efficiently and release it on demand to maintain the cabin temperature, reducing the dependence on the vehicle's internal heating system, and have accordingly been employed in several studies to reduce the heating load on the EV battery and to improve thermal comfort under cold weather conditions [15, 16]. However, despite the advantages of PCMs for use in the thermal management of EVs' batteries, the low thermal conductivity of PCMs (0.2 to 2 $W\ m^{-1}\ K^{-1}$) hampers their large-scale application. Thermal energy storage for electrified vehicles operating at low ambient temperatures has been comprehensively reviewed by Xie et al. [17], covering system concepts, storage devices and candidate materials. Based on field measurements reported by Knote et al. [18], the specific energy consumption of electric buses can nearly double under sub-zero conditions compared with temperate operation, mainly due to the increased cabin heating requirement. Similarly, Kuitunen et al. [19, 20] have developed a high-speed charging thermal energy storage system using paraffin-based PCM for urban electric buses. The system is designed to keep the cabin temperature around 18°C and can be thermally charged in minutes using a high-voltage terminal charger. These findings show that thermal loads constitute a significant share of the total energy consumption of FCEVs, particularly under cold ambient conditions. This underlines the potential of recovering the powertrain waste heat, and motivates the PCM-based thermal energy storage approach investigated in this study.

Although PCM-based thermal energy storage has been extensively studied for battery thermal management in PEVs and buses, system-level studies that integrate fuel cell waste heat recovery, PCM-based thermal storage, and cabin heating in a fuel cell hybrid vehicle remain scarce. To address this gap, the present study develops an integrated vehicle thermal management model of the second-generation Toyota Mirai, in which the fuel cell stack, electric motor, battery, cabin, and a PCM storage unit are simulated simultaneously over the worldwide harmonized light vehicle test cycle (WLTC) Class 3 cycle under summer and winter conditions. The main novelty of this work is the quantification of the contribution of a pre-charged PCM unit to cold-start cabin heating, PTC power reduction, and hydrogen consumption against a baseline without PCM, using an integrated system-level model whose hydrogen consumption prediction is verified against the certified WLTP value of the vehicle.

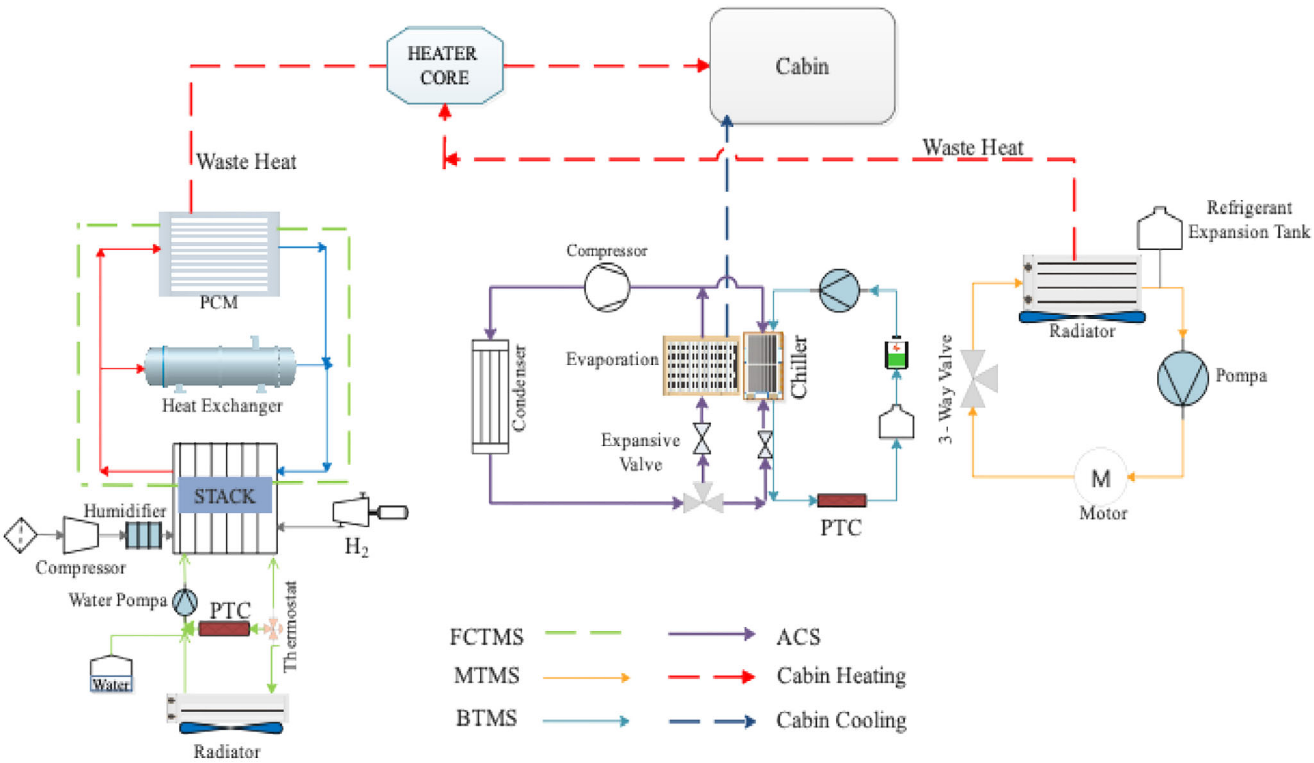

FIGURE 1 | Schematic overview of the vehicle thermal management system (VTMS).

2 | VTMS System

2.1 | System Description

The integrated vehicle thermal management system (VTMS) considered in this study is developed for a fuel cell hybrid electric vehicle (FCHEV) and is designed to ensure the safe, efficient, and energy-optimal operation of all thermally sensitive subsystems. In this study, the second-generation Toyota Mirai is adopted as the reference vehicle, in which the relatively small lithium-ion battery pack is not intended to serve as the primary energy source but rather to support the fuel cell system under transient power demand conditions. Accordingly, the VTMS architecture integrates the thermal management of the fuel cell stack, battery pack, electric motor, and cabin within a coordinated framework.

The VTMS architecture has four major thermal systems: FCTMS, BTMS, MTMS, and ACS. The new design for VTMS also includes an energy storage device made up of PCM. The purpose of the device is to improve the process of utilizing waste heat from the fuel cell stack and motor. The FCTMS and BTMS manage the fuel cell stack and battery pack, respectively, to ensure that each component operates at its optimal and safe temperature range, providing reliable power production and reducing thermal degradation (Figure 1). Meanwhile, the MTMS controls the thermal profile of the electric motor and power electronics system, and the ACS regulates the cabin temperature toward the desired set-point. Hydrogen is stored on board in three Type-IV composite tanks at a nominal pressure of 700 bar, and the supply pressure is regulated down to approximately 1.6 bar at the stack inlet. In the suggested VTMS design, R1234yf refrigerant is utilized in the ACS of the vehicle to provide cabin cooling and auxiliary thermal connection, while an ethylene glycol coolant is used in the fluidic circuit of the fuel cell and motor thermal systems. Unlike the fuel cell and motor, the relatively small lithium-ion battery pack of the Toyota Mirai is considered in the air-based battery thermal management design, where cabin air is used as the thermal medium for the battery. To improve cold-starting and winter performance, a positive temperature coefficient (PTC) heater is incorporated into the BTMS as a supplemental battery warming mechanism. The PTC heater works when the vehicle starts in cold conditions or when the ambient temperature is low during winter. Its role is to ensure that the lithium-ion battery, which is comparatively smaller and uses an air cooling mechanism, is heated up to a suitable operating temperature. Under actual driving conditions, the fuel cell stack will get hotter compared to the battery. As such, cooling for the fuel cell stack is done using a liquid coolant consisting of ethylene glycol water. The recovered heat from the fuel cell stack and the electric motor drives a PCM thermal storage device, which heats the passenger compartment in cold weather. The PCM is packaged as an insulated storage tank, and the heat exchanger shown beneath it in Figure 1 provides the thermal exchange between the FC coolant (working fluid) and the PCM. The electric motor and the controller operate at a broad temperature range. However, their main requirement is cooling rather than heating. Therefore, temperature-based control is recommended for the VTMS (refer to Figure 2).

The PCM component is designed as an insulated storage tank, and the heat exchanger shown directly beneath it provides the thermal exchange between the FC coolant (working fluid) and the PCM.

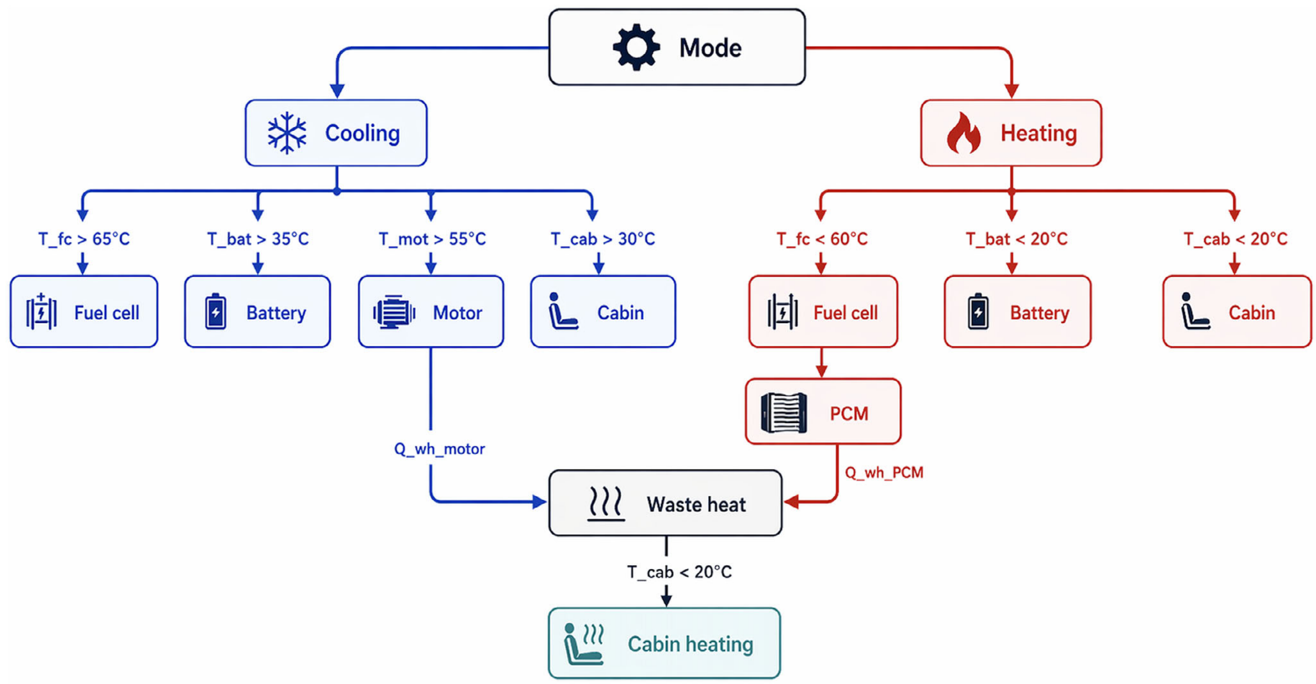

FIGURE 2 | Operational diagram of the vehicle thermal management system under heating and cooling modes.

3 | System Modelling

3.1 | VTMS Model Description

A comprehensive model of the VTMS for a FCHEV is developed in this study. The proposed VTMS framework integrates all thermally and energetically coupled subsystems to accurately capture the interactions between power generation, waste heat recovery, and cabin heating and cooling loads. The overall system model includes a vehicle dynamics model, a fuel cell model, a PCM-based thermal energy storage model, a battery model, an electric motor model, and an ACS model.

3.1.1 | Vehicle Specifications

The vehicle model is parameterized using the technical data of the second-generation Toyota Mirai [4]. The basic characteristics, such as vehicle mass, frontal area, aerodynamic coefficient of friction, rolling resistance, and drivetrain characteristics, are summarized in Table 1. These parameters are based on the WLTC Class 3 driving cycle to determine the traction force demand and Vehicle speed input, while the hydrogen consumption result is verified according to the official WLTP-based reference value of the Toyota Mirai. The main vehicle parameters are also summarized in Table 1.

3.1.2 | Modeling of PEMFC

To calculate the heat generated by the fuel cell stack, it is assumed that the chemical energy released during the electrochemical reactions is converted into electrical output and thermal losses. Based on this assumption, the instantaneous heat generation power of the fuel cell stack can be expressed as [21–23]

TABLE 1 | Specifications of the vehicle [4].

Parameter	Value
Vehicle length (mm)	4975
Vehicle width (mm)	1885
Vehicle height (mm)	1470
Curb weight (kg)	1950
Rolling resistance coefficient	0.010
Aerodynamic drag coefficient, (C_D)	0.29
Wheelbase length (m)	2.92
Maximum vehicle speed (km/h)	175
Maximum grade (%)	20
Overall powertrain efficiency	0.90

$$V_{\text{cell}} = E_{\text{Nernst}} - V_{\text{act}} - V_{\text{ohm}} - V_{\text{con}} \tag{1}$$

$$E_{\text{Nernst}} = 1.229 - (0.85 \times 10^{3}) \times (T_{\text{cell}} - T_{\text{ref.}}) + (4.3085 \times 10^{-5}) \times T_{\text{cell}}[\ln(P_{H_2}) + 0.5 \times \ln(P_{O_2})] \tag{2}$$

$$V_{\text{act}}^{\text{an}} = \frac{RT}{\alpha_{\text{an}} F} \ln \frac{i}{i_0^{\text{an}}} \tag{3}$$

$$V_{\text{act}}^{\text{cat}} = \frac{RT}{\alpha_{\text{cat}} F} \ln \frac{i}{i_0^{\text{can}}} \tag{4}$$

TABLE 2 | Key parameters of the vehicle and thermal subsystems [4].

Subsystem	Parameter	Unit	Value
	Rated power	kW	128
	Efficiency	—	0.55
Fuel cell	Nominal operating temperature	°C	75–80
	Mass	kg	52
	Number of cell	—	330
	Nominal power	kW	134
	Maximum torque	Nm	300
Motor	Efficiency	—	0.93
	Optimal temperature	°C	55
	Mass	kg	80
	Target cabin temperature	°C	22
Cabin	Number of occupants	—	4
	Heat per occupant	W	90
	Disable temperature	°C	20
	Maximum compressor power	kW	6
PTC	Nominal COP	—	2.8
	Refrigerant	—	R1234yf
	Coolant	—	Ethylene glycol
ACS	Cabin target temperature	°C	22
	Maximum condenser temperature	°C	50

$$V_{ohm} = V_{act}^{el} + V_{act}^{pl} + V_{act}^{mem} = (R_{el} + R_{pl} + R_{mem}) I_{cell} \quad (5)$$

It should be noted that the interfacial contact resistances between the fuel cell components (e.g., between the gas diffusion layers and the bipolar plates) are not treated as separate terms in Equation (5); they are implicitly lumped into the equivalent electrode and bipolar plate resistances. This simplification is consistent with the system-level scope of the present study, in which the stack electrical performance is represented by a load-dependent efficiency map calibrated against the published peak efficiency of the Toyota Mirai Gen2 stack, so that all resistive loss mechanisms are inherently reflected in the resulting efficiency characteristics.

$$V_{con} = \frac{RT}{2F} \ln \frac{C_{H_2}^{mem}}{C_{H_2,0}^{mem}} + \frac{RT}{4F} \ln \frac{C_{O_2}^{mem}}{C_{O_2,0}^{mem}} \quad (6)$$

$$P_{sta} = (V_0 \times V_{cell}) \times I_{cell} \times N \quad (7)$$

$$I_{cell} = A_{stack} \times i \quad (8)$$

where P_{sta} denotes the instantaneous heat generation power of the stack, V_0 represents the reference voltage of a single cell, V_{cell} is the instantaneous voltage of an individual cell, I_{cell} is the stack current, N is the total number of cells in the stack, i is the current density, and A_{stack} is the active area of the fuel cell stack. The rated power of the fuel cell in this work is 128 kW; the key parameters of the vehicle and its thermal subsystems are summarized in Table 2. Activation losses occur due to the oxidation and reduction reactions within the fuel cell; these losses are exacerbated by the slow reaction rates at the electrodes, whilst a portion of the total voltage generated by the fuel cell is consumed in driving the chemical reactions [24].

TABLE 3 | Parameters of the battery pack [4].

Parameter	Value
Type	Lithium-ion
Nominal voltage (V)	310.8
Battery pack Capacity (Ah)	4.0
Package weight (kg)	44.6

3.1.3 | Battery Pack Mode

The battery serves as an auxiliary energy source in the fuel cell vehicle and plays a significant role in meeting the transient power demand of the vehicle. In this study, a lithium-based battery pack is considered, which is widely adopted in electric and hybrid vehicles due to its high safety, long cycle life, and cost-effectiveness. The battery operates within a safe temperature range of approximately 20°C–45°C, and its main specifications are listed in Table 3. During vehicle operation, the battery inevitably generates heat as electrical energy is delivered or

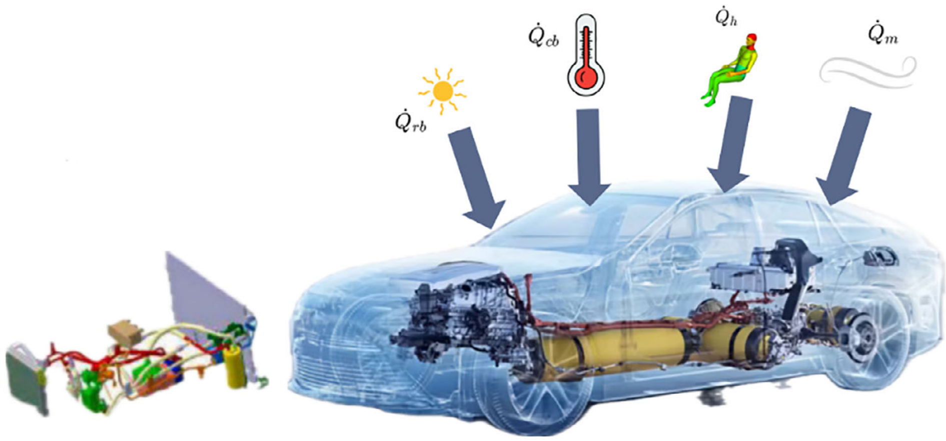

FIGURE 3 | Cabin thermal model schematic for the hydrogen fuel cell vehicle.

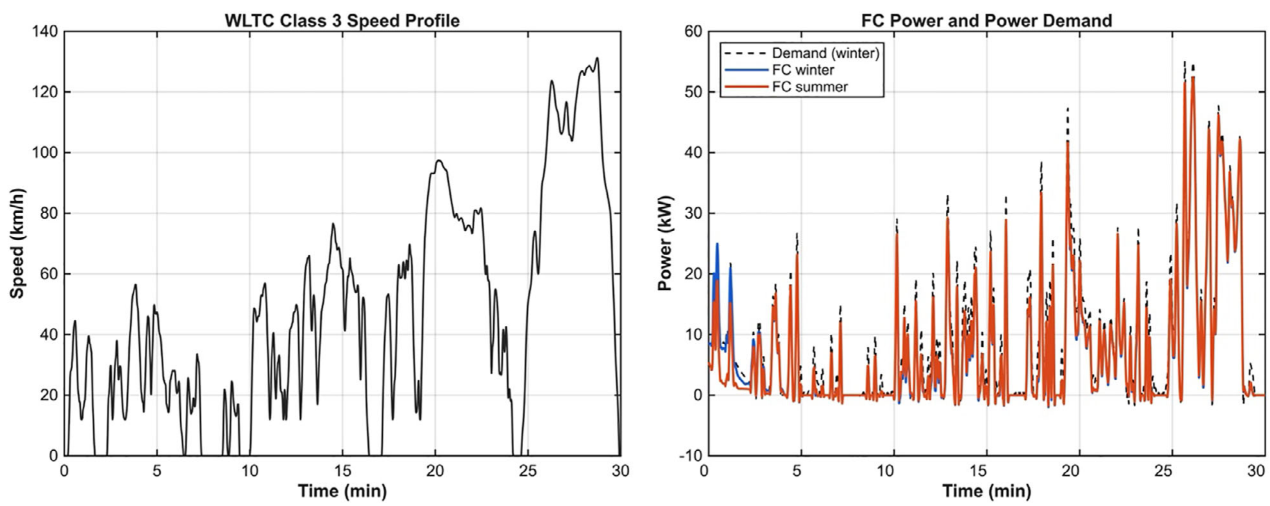

(a) (b)

FIGURE 4 | WLTC Class 3 driving cycle: (a) speed profile, (b) fuel cell power and total electrical power demand.

absorbed. In practical battery systems, heat generation originates from several mechanisms, including internal resistance losses, electrochemical reactions, polarization effects, and side reactions. Among these, internal resistance losses represent the dominant contribution under high-power and long-duration operating conditions, which are typical for FCHEVs. The battery is modeled as an auxiliary energy source in the FCHEV. Battery heat generation is simulated as an internal-resistance loss based on the current calculated from the nominal battery voltage.

$$I_{\text{bat}} = P_{\text{bat}} \,/\, V_{\text{bat}} \tag{9}$$

where P_{bat} refers to the battery power and V_{bat} is the nominal battery voltage.

Computing the current from the nominal voltage, instead of solving it from the open-circuit voltage and the internal resistance, is a common system-level simplification and is consistent with the narrow SOC window in which the pack is operated, where the terminal voltage remains close to its nominal value. The heat generation of the battery pack is therefore evaluated using an ohmic loss model [25]:

$$Q_{\text{bat}} = I^2_{bat.} \cdot R_{\text{int}} - I_{\text{bat}} T_{\text{bat}} \frac{dV_{\text{oc}}}{dT_{\text{bat}}} \tag{10}$$

where Q_{bat} denotes the battery heat generation rate, $I_{\text{bat.}}$ is the battery current, and R_{int} is the equivalent internal resistance of the battery. The temperature-dependent open-circuit voltage and entropic heat terms are neglected in this study in order to maintain consistency with the system-level modelling framework and to reduce computational complexity. The state of charge is updated at each time step from the net battery power:

$$\text{SOC}\,(t + \Delta t) = \text{SOC}\,(t) \;-\; (P_{\text{bat}} \;\cdot\; \Delta t) \;/\; E_{\text{nom}} \tag{11}$$

where P_{bat} is positive during discharge and negative during charging, and $E_{\text{nom}} = 3600 \cdot V_{\text{nom}} \cdot C_{\text{Ah}}$ is the nominal pack energy (≈1.24 kWh). The SOC is initialized at 0.55 and constrained to 0.30–0.80.

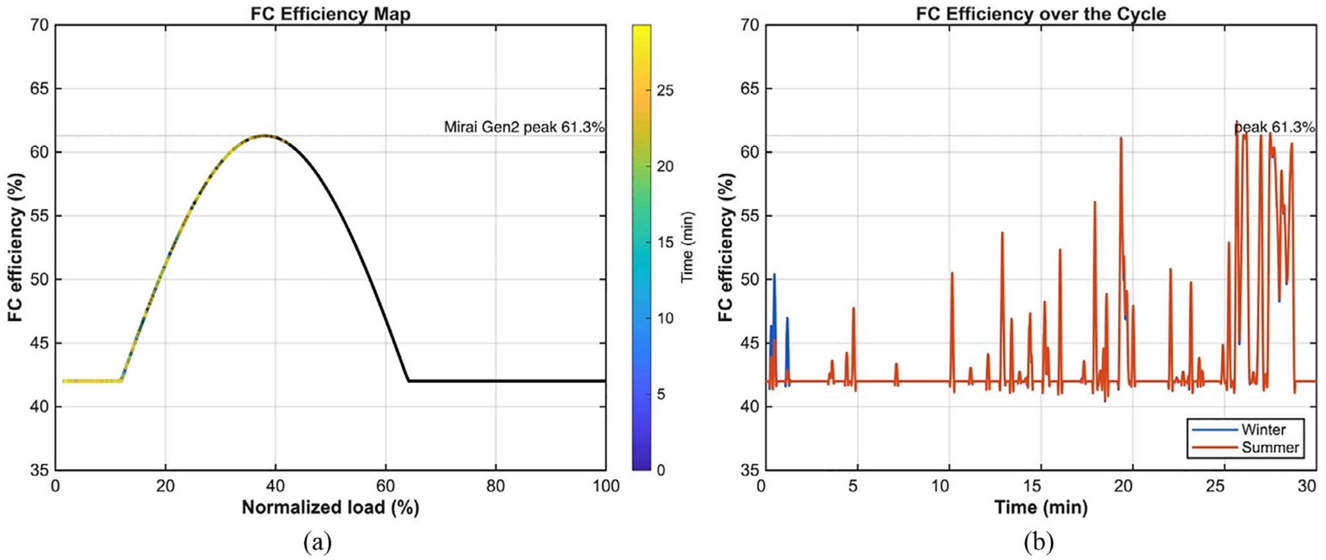

FIGURE 5 | Fuel cell efficiency: (a) load-dependent efficiency map calibrated to the Mirai Gen2 peak efficiency of 61.3%, with winter operating points, (b) instantaneous efficiency over the cycle.

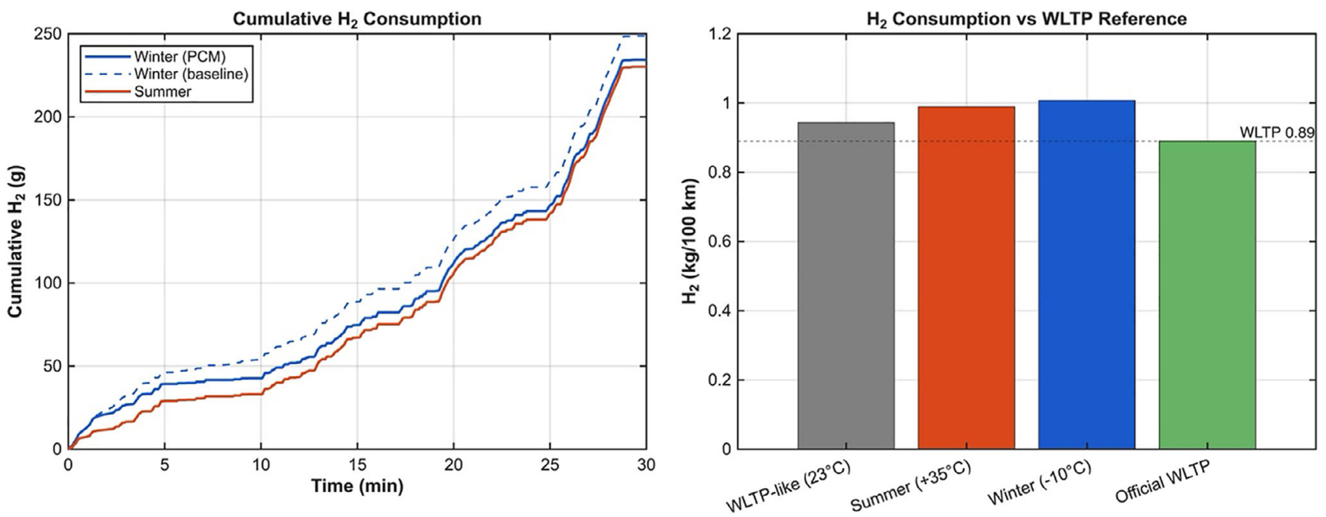

FIGURE 6 | Hydrogen consumption validation: (a) cumulative consumption (winter with/without PCM, summer), (b) comparison with the official WLTP reference value.

3.1.4 | Vehicle Longitudinal Dynamics and Power Demand Model

The powertrain model plays a critical role in determining the electric motor load and the corresponding electrical power demand, which directly influences the energy management strategy and thermal behavior of the vehicle. Key powertrain parameters, including the main reduction ratio and drivetrain efficiency, are summarized in Table 1.

Rolling resistance force:

$$F_{\text{roll}} = m \cdot g \cdot f_{\text{roll}} \tag{12}$$

Aerodynamic drag force:

$$F_{\text{aero}} = 0.5 \cdot \rho_{\text{air}} \cdot C_D \cdot A_{\text{front}} \cdot u^2 \tag{13}$$

Inertial force:

$$F_{\text{in}} = m \cdot a \tag{14}$$

Total tractive force and wheel power:

$$F_{\text{total}} = F_{\text{roll}} + F_{\text{aero}} + F_{\text{in}} \tag{15}$$

$$P_{\text{wheel}} = F_{\text{total}} \cdot u \tag{16}$$

Motor shaft power (considering efficiency) [26]:

$$P_{\text{mot}} = max(0,\ P_{\text{wheel}} \,/\, \eta_{\text{pt}} \tag{17}$$

where m is the vehicle mass, g is the gravitational acceleration, f_{roll} is the rolling resistance coefficient, ρ_{air} is the air density, C_D is the aerodynamic drag coefficient, A_{front} is the vehicle frontal area, u is the vehicle speed, a is the longitudinal acceleration. The electric motor shaft power is calculated by considering the powertrain efficiency:

The electrical power required to drive the motor is:

$$P_{\text{drive}} = P_{\text{motor}} / \eta_{\text{motor}} \tag{18}$$

The total electrical demand of the vehicle, including auxiliary systems, is given by:

$$P_{\text{dem.}} = P_{\text{PTC}} + P_{\text{drive}} + P_{\text{comp.}} \tag{19}$$

where P_{PTC} represents the power consumption of the battery PTC heater and $P_{\text{comp.}}$ denotes the compressor power of the air-conditioning system.

3.1.5 | Waste Heat Generation

The waste heat generated by the fuel cell stack is calculated from the instantaneous, load-dependent stack efficiency η_{fc}

$$Q_{(\text{fc,waste})} = P_{\text{fc}} \cdot (1 - \eta_{\text{fc}}) / \eta_{\text{fc}} \tag{20}$$

where P_{fc} is the net electrical output power of the stack.

Similarly, the waste heat generated by the electric motor is expressed as:

$$Q_{\text{motor,waste}} = P_{\text{motor}} \cdot (1 - \eta_{\text{motor}}) \tag{21}$$

Accordingly, the total available waste heat in the system is given by:

$$Q_{\text{waste,total}} = Q_{\text{fc,waste}} + Q_{\text{motor,waste}} \tag{22}$$

3.1.6 | PCM Thermal Energy Storage Model

A thermal energy storage module based on PCM was implemented in the Toyota Mirai Gen2 FCHEV model to buffer the irregular waste heat produced by the proton exchange membrane fuel cell (PEMFC) stack and provide additional cabin heat during cold-start and low-load operating conditions. PCMs take advantage of high latent heat of fusion associated with solid-liquid phase transition at approximately isothermal temperature, so that heat generation is decoupled from heat demand in time [14, 27]. For the vehicular FCHEV applications, paraffin-based or fatty-acid-based PCMs melting in the range 50°C–60°C [28] are especially attractive because of their chemical stability, non-corrosiveness and compatibility with the typical FC coolant temperature operating window (55°C–90°C) [29, 30]. In the winter scenario, the PCM is assumed to be fully charged at trip start, representing waste heat stored during the preceding drive and retained in the insulated tank; it is subsequently recharged by the FC coolant whenever surplus waste heat is available.

TABLE 4 | Thermophysical properties of the PCM used in the simulation [32].

Parameter	Symbol	Unit	Value
Solid-phase specific heat	$c_{p,s}$	J kg^{-1} K^{-1}	1800
Liquid-phase specific heat	$c_{p,l}$	J kg^{-1} K^{-1}	2400
Latent heat of fusion	L	J kg^{-1}	200 000
Lower melting temperature	$T_{m,L}$	°C	53.0
Upper melting temperature	$T_{m,H}$	°C	54.5

The PCM is modeled using the effective enthalpy method [27, 31], in which the stored thermal energy is expressed as a function of temperature. The thermophysical properties of the selected PCM are summarized in Table 4.

3.1.7 | Integrated and Cabin HVAC Thermal Model

Cabin air conditioning constitutes a major auxiliary load in FCEVs, competing directly with the traction energy demand, particularly under winter conditions where the heating requirement is highest. Accordingly, a lumped-parameter cabin thermal sub-model is developed and coupled to the overall FCHEV energy management model, so that the cabin heating and cooling loads are computed consistently with the waste heat availability of the powertrain. All heat flows illustrated in Figure 3 act on the cabin of a real vehicle. In the present lumped-parameter model, these inputs are represented at different levels of detail: the occupant heat gain is included as a constant term, the envelope conduction and air-leakage losses are lumped together into a single effective coefficient and the cabin is assumed to operate in recirculation mode, so that no additional fresh-air ventilation load arises. The solar radiation input is neglected; this is a conservative assumption for the winter heating case, which is the focus of this study, since solar gains would reduce the heating demand, whereas in summer it leads to a slight underestimation of the cooling load.

4 | Results and Discussion

4.1 | Model Validation

To evaluate the accuracy and reliability of the developed vehicle thermal management and energy allocation models, comprehensive simulation tests were conducted under the WLTC Class 3 driving cycle. The WLTC Class 3 cycle was selected for three reasons. First, the official hydrogen consumption of the Toyota Mirai (0.89 kg/100 km) is homologated under the WLTP procedure; simulating the same cycle therefore allows a direct validation of the model against the manufacturer's certified value. Second, the WLTC Class 3 cycle applies to vehicles with a power-to-mass ratio above 34 W/kg and a maximum speed above 120 km/h, which matches the performance characteristics of the Mirai Gen2 (maximum speed 175 km/h); the extra-high phase of the cycle, reaching approximately 131 km/h, is therefore representative of the vehicle's actual high-speed capability. Third, the cycle covers low, medium, high and

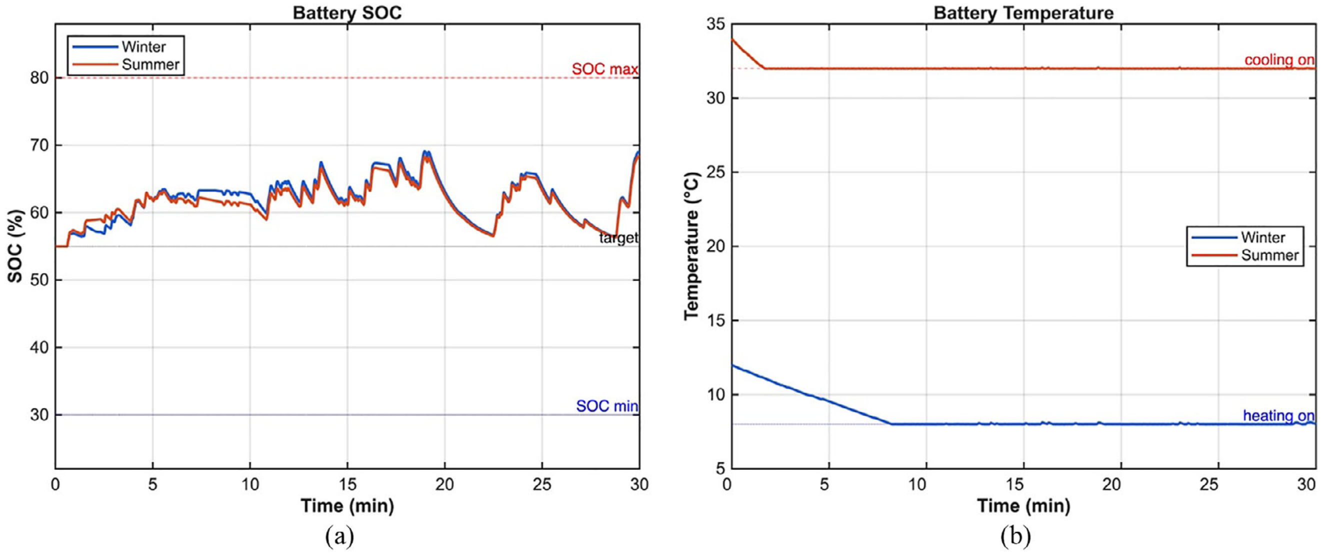

FIGURE 7 | Battery response: (a) state of charge, (b) temperature with cooling/heating thresholds.

extra-high speed phases, providing representative transient traction loads and waste-heat generation conditions for the evaluation of the TMS. Figure 4 shows the speed profile of the cycle together with the resulting fuel cell power and total electrical power demand; the total driving distance is 23.26 km in all cases.

Figure 5a shows the load-dependent efficiency map of the Toyota Mirai Gen2 stack, calibrated against reference data (maximum net efficiency 61.3%), together with the instantaneous operating points of the winter simulation; Figure 5b presents the resulting efficiency over the cycle. Since the WLTC contains long low-load phases, the time-weighted mean efficiency (44.9%) is considerably lower than the energy-weighted mean efficiency (48.7% in summer and 48.5% in winter), the latter being the metric relevant to hydrogen consumption.

The hydrogen consumption validation is presented in Figure 6. Since the official WLTP figure of the Toyota Mirai is homologated with the air conditioning inactive [4], an additional WLTP-like reference case (23°C ambient, negligible HVAC load) was simulated for validation purposes. The predicted consumption of this case is 0.944 kg/100 km, within 6.0% of the certified value of 0.89 kg/100 km, which is considered acceptable for a system-level model of this scope. Under seasonal HVAC loads, the consumption increases to 0.989 kg/100 km at +35°C and to 1.007 kg/100 km at −10°C (with PCM), reflecting the additional compressor and heating loads discussed in Sections 4.2–4.4.

4.2 | Energy and Powertrain Results

The total hydrogen consumption over the cycle is 0.230 kg in summer and 0.234 kg in winter with the PCM unit, compared with 0.249 kg for the winter baseline without PCM. The battery state of charge is shown in Figure 7a. Starting from 55%, the SOC rises to 68.2% in summer and 69.0% in winter, with a variation range of 13%–14%, confirming a dynamic battery model. The recovered regenerative braking energy is 1089.5 Wh in both seasons (Figure 8b) and is the main driver of the net SOC increase; the SOC-based load-following controller returns the fuel cell to its minimum sustaining power whenever the SOC exceeds the 55% target. A tighter SOC regulation strategy is identified as a possible refinement. The battery temperature response is discussed in Section 4.3. The motor remains thermally uncritical throughout the cycle (Figure 8a), reaching 43.4°C in summer and 27.0°C in winter.

4.3 | 4.3 Component Thermal Management

The fuel cell thermal response is shown in Figure 9a. The stack temperature rises from 35.0°C to 79.5°C in summer and from 22.0°C to 80.2°C in winter, that is, to the nominal PEMFC operating point of 75°C–80°C. This behavior is intended: during cold-ambient operation the thermostat/three-way valve restricts radiator flow (Figure 9b) so that the stack warms up quickly and the waste heat is preserved for useful thermal loads; the valve begins to open only after the coolant temperature increases. The coolant reaches 54.4°C in summer and 55.3°C in winter, remaining below the stack temperature due to the stack-to-coolant thermal resistance and the heat extracted for cabin heating, PCM charging and radiator rejection.

The battery temperature (Figure 7b) decreases from 34.0°C to 32.0°C in summer, where the refrigerant chiller prevents the pack from exceeding the 32°C cooling threshold. In winter, the pack cools from 12.0°C to the 8°C heating threshold, at which point the 1.5 kW battery heater maintains the temperature at the lower limit of the preferred operating window.

4.4 | Cabin Heating, PCM, and Waste Heat Recovery Performance

The PCM state and the cabin temperatures are shown in Figure 10. In the winter scenario the PCM starts pre-charged

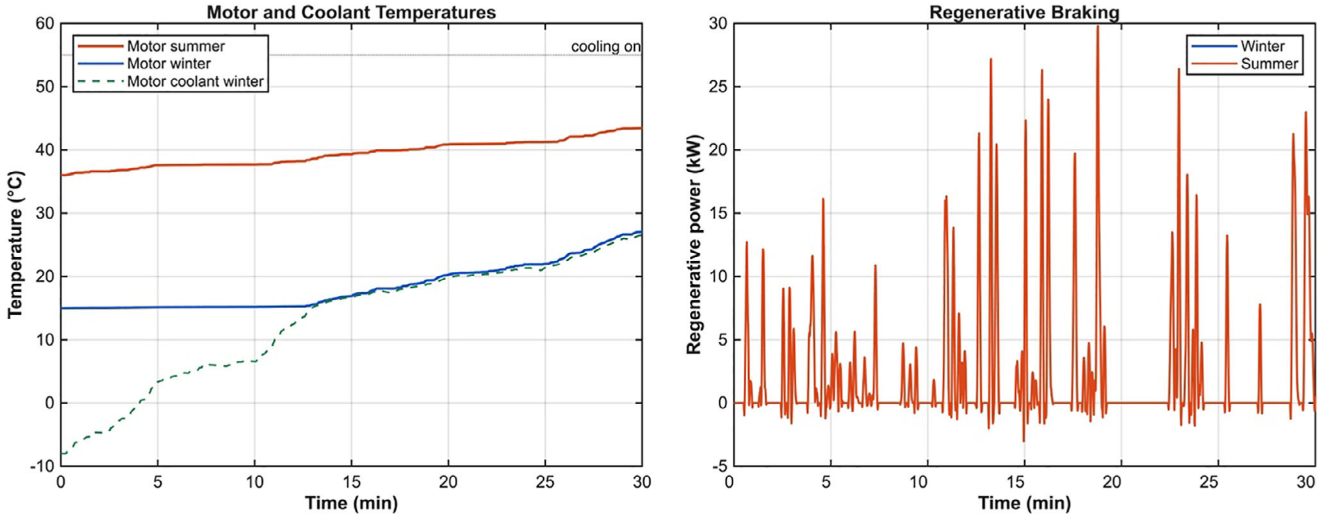

(a) (b)

FIGURE 8 | (a) Motor and motor coolant temperatures, (b) regenerative braking power.

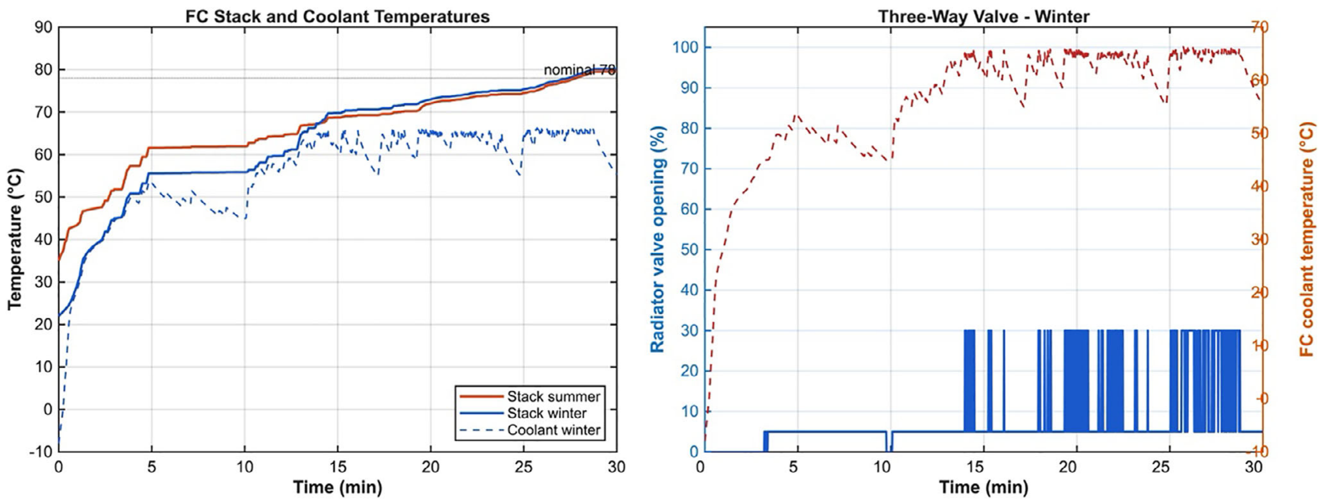

(a) (b)

FIGURE 9 | Fuel cell thermal management: (a) stack and coolant temperatures, (b) three-way valve opening and coolant temperature (winter).

(55.5°C, SOC = 1), representing waste heat stored during the preceding drive in the insulated tank. During the cold start it discharges along its melting plateau and ends the cycle at 53.1°C with 31% of its capacity remaining. The cabin warms from –10°C to 15.0°C within the 30-min cycle; the comparison with the no-PCM baseline in Figure 10b shows a markedly faster initial warm-up. The cabin does not reach the 22°C target within the short cycle, which is attributed to the heater-core capacity and the cycle duration rather than to the storage itself; the role of the PCM is to bridge the cold-start phase until the fuel cell waste heat becomes available.

The winter heating source hierarchy is shown in Figure 11a and the corresponding energy distribution in Figure 11b. Over the full cycle the PCM supplies 1204 Wh to the cabin, the fuel cell 66 Wh, the motor 38 Wh and the PTC heater 156 Wh. During the first 10 min of the cold start, the PCM alone provides 525 Wh, corresponding to 73.9% of the delivered cabin heat in this phase. Compared with the no-PCM baseline — in which the fuel cell supplies 968 Wh and the PTC 375 Wh — the PCM reduces the PTC consumption by 219 Wh (58.4%) and the hydrogen consumption by 14.3 g (5.8%). The hydrogen saving is energy-consistent: 219 Wh of avoided electric heating at the prevailing stack efficiency corresponds to approximately 13.5 g of hydrogen.

The overall winter waste heat recovery is illustrated in Figure 12a: 29.2% of the total powertrain waste heat (1308 Wh of 4473 Wh) is recovered for useful heating and storage. In summer (Figure 12b), the improved air-conditioning model pulls the cabin down from 35°C and holds it near 26°C, in line with the recirculation assumption and the treatment of the cabin heat flows described in Section 3.1.7.

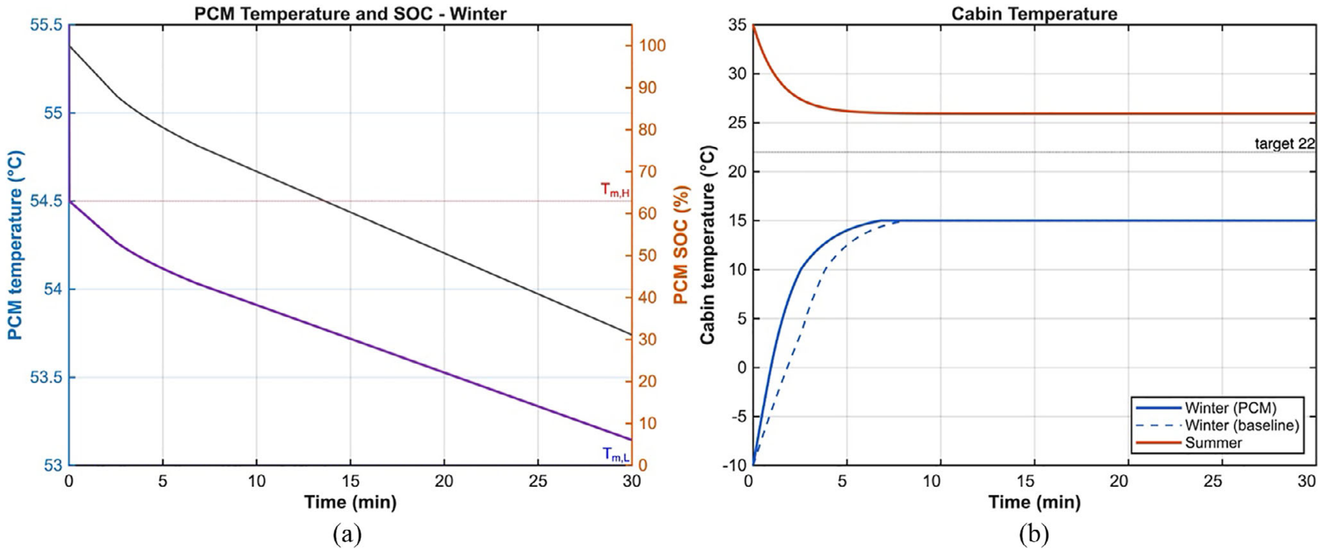

FIGURE 10 | (a) PCM temperature and state of charge (winter), (b) cabin temperature (winter with/without PCM, summer).

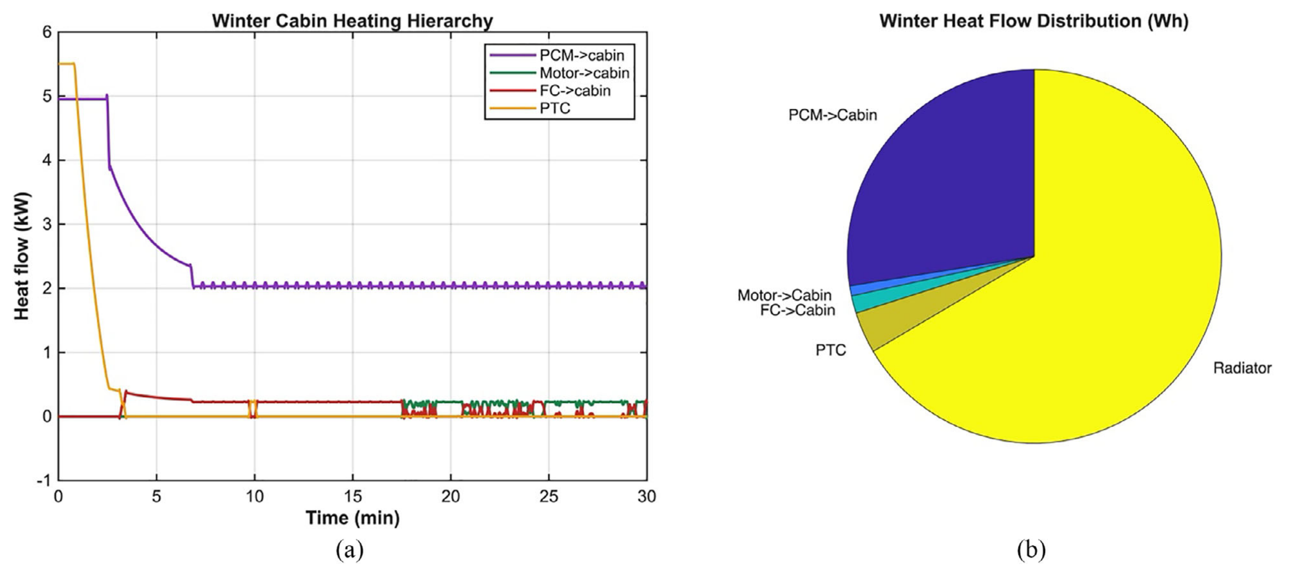

FIGURE 11 | Winter cabin heating: (a) source hierarchy (PCM, motor, FC, PTC), (b) heat flow distribution.

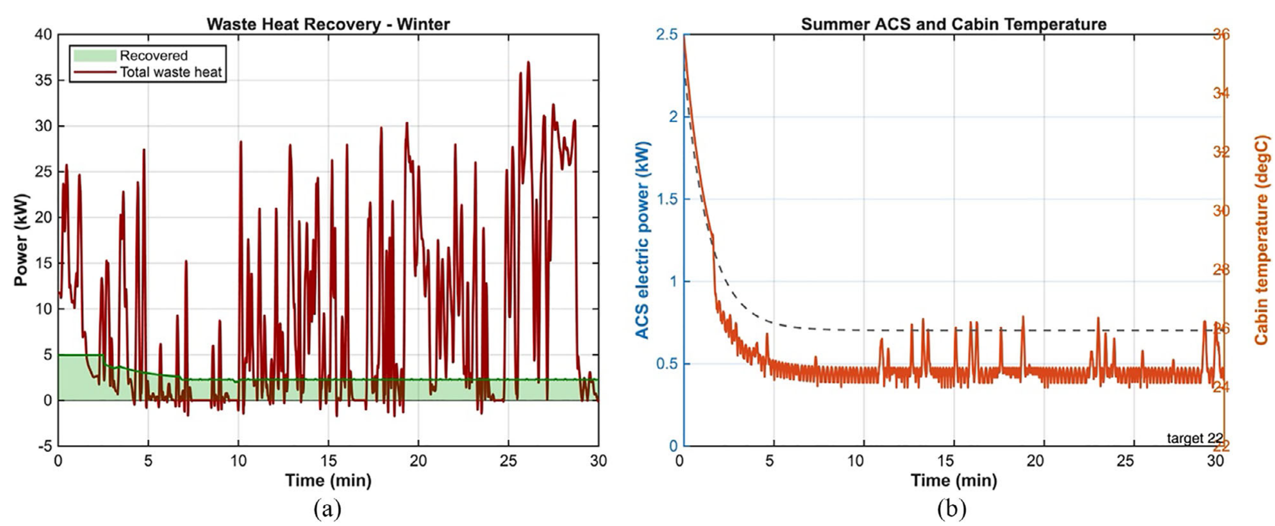

FIGURE 12 | (a) Winter waste heat generation and recovery, (b) summer ACS power and cabin temperature.

5 | Conclusions and Future Work

In this study, a WLTC-based simulation model of the second-generation Toyota Mirai was developed to evaluate hydrogen consumption and thermal management performance under summer (+35°C) and winter (−10°C) conditions. The model couples the fuel cell stack, high-voltage battery, electric motor, cabin, radiator circuits, PTC heaters, and a PCM thermal energy storage unit, and every scenario was additionally simulated without the PCM to isolate its contribution.

Under WLTP-like conditions (23°C, air conditioning inactive), the simulated hydrogen consumption is 0.944 kg/100 km, within 6% of the certified value of 0.89 kg/100 km. Seasonal HVAC loads raise the consumption to 0.989 kg/100 km in summer and 1.007 kg/100 km in winter. The stack reaches its nominal operating point in both seasons (79.5°C and 80.2°C), maintained by the three-way valve strategy that restricts radiator flow during warm-up. The battery SOC rises from 55% to about 69% over the cycle, driven mainly by the 1089 Wh of recovered braking energy; a tighter SOC regulation around the target value remains a point for refinement.

The central finding concerns the PCM unit. Operated as a precharged thermal storage holding the waste heat of the preceding drive in its insulated tank the 28 kg paraffin unit (melting range 53°C–54.5°C) supplied 1204 Wh of cabin heat over the winter cycle and covered 73.9% of the delivered heating during the first 10 min of the cold start, precisely the phase in which the fuel cell cannot yet provide useful waste heat. Compared with the baseline without PCM, the electric PTC consumption dropped by 219 Wh (58.4%) and the hydrogen consumption by 5.8%. Together with the direct use of fuel cell and motor waste heat, 29.2% of the total powertrain waste heat was recovered for useful purposes. The cabin warmed from –10°C to 15°C within the 30-min cycle; reaching the 22°C setpoint would require either a longer trip or a larger heater-core capacity and is a matter of component sizing rather than a limitation of the storage concept itself.

A PMV/PPD-based thermal comfort assessment, a calibrated efficiency map based on experimental polarization data, and an optimization of the PCM mass and heat exchanger conductance for different trip lengths are planned as the next steps.

Nomenclature

i	current density (A cm^{-2})
I	current (A)
m	mass (kg)
PH_2	partial pressure of hydrogen
PO_2	partial pressure of oxygen
W	power
R_{el}	resistances of the electrodes
R_{mem}	resistances of the membrane
R_{pl}	resistances of the bipolar plates
T	temperature (°C)
V	voltage (V)
E_{Nernst}	reversible voltage overpotential
P_a	pressures of the anode
P_c	pressures of the cathode
$Q_{fc,waste}$	waste heat generated by the fuel cell stack
R_{int}	equivalent internal resistance of the battery
V_{act}	activation overpotential
V_{con}	concentration overpotential
V_{ohm}	ohmic overpotential

Subscripts

bat	battery
comp	compressor
mem	membrane

Data Availability Statement

The data that support the findings of this study are available from the corresponding author upon reasonable request.

References

1. D. Yağcı, H. Genceli, and O. E. Turgut, "Guided Manta Ray Foraging Optimization for Accurate Parameter Extraction of PEM Fuel Cell," *Fuel Cells* 26 (2026): e70077, https://doi.org/10.1002/fuce.70077.

2. W. C. Yang, B. Bates, N. Fletcher, and R. Pow, "Control Challenges and Methodologies in Fuel Cell Vehicle Development," SAE Technical Paper 98C054, Presented at the 1998 International Congress on Transportation (Electronics Convergence Transportation Electronics Association, 1998) 1–10.

3. Y. Zhang, C. Zhang, Z. Huang, L. Xu, Z. Liu, and M. Liu, "Real-Time Energy Management Strategy for Fuel Cell Range Extender Vehicles Based on Nonlinear Control," *IEEE Transactions on Transportation Electrification* 5 (2019): 1294–1305, https://doi.org/10.1109/TTE.2019.2958038.

4. Toyota, "Toyota Mirai Technical Specifications," 2022, https://media.toyota.co.uk/wp-content/uploads/sites/5/pdf/220203M-Mirai-Tech-Spec.pdf.

5. E. Alpaslan, M. U. Karaoğlan, and C. O. Colpan, "Investigation of Drive Cycle Simulation Performance for Electric, Hybrid, and Fuel Cell Powertrains of a Small-Sized Vehicle," *International Journal of Hydrogen Energy* 48 (2023): 39497–39513, https://doi.org/10.1016/j.ijhydene.2023.08.358.

6. S. Tsushima, K. Teranishi, and S. Hirai, "Magnetic Resonance Imaging of the Water Distribution Within a Polymer Electrolyte Membrane in Fuel Cells," *Electrochemical and Solid-State Letters* 7 (2004): A269, https://doi.org/10.1149/1.1774971.

7. Z. Wei, R. Song, D. Ji, Y. Wang, and F. Pan, "Hierarchical Thermal Management for PEM Fuel Cell With Machine Learning Approach," *Applied Thermal Engineering* 236 (2024): 121544, https://doi.org/10.1016/j.applthermaleng.2023.121544.

8. L. Li, S. Gao, B. Wang, et al., "Analysis of Cooling and Heating Characteristics of Thermal Management System for Fuel Cell Bus," *International Journal of Hydrogen Energy* 48 (2023): 11442–11454, https://doi.org/10.1016/j.ijhydene.2022.07.083.

9. Z. Rao and S. Wang, "A Review of Power Battery Thermal Energy Management," *Renewable and Sustainable Energy Reviews* 15 (2011): 4554–4571, https://doi.org/10.1016/j.rser.2011.07.096.

10. E. Akram, *Aging Modeling and Determination of the State of Health of Lithium-Ion Batteries for Electric and Hybrid Vehicle Applications* (University of Bordeaux, 2013).

11. M. Malik, I. Dincer, and M. A. Rosen, "Review on Use of Phase Change Materials in Battery Thermal Management for Electric and Hybrid Electric Vehicles," *International Journal of Energy Research* 40 (2016): 1011–1031, https://doi.org/10.1002/er.3496.

12. X. M. Xu and R. He, "Review on the Heat Dissipation Performance of Battery Pack With Different Structures and Operation Conditions," *Renewable and Sustainable Energy Reviews* 29 (2014): 301–315, https://doi.org/10.1016/j.rser.2013.08.057.

13. T. M. Bandhauer, S. Garimella, and T. F. Fuller, "A Critical Review of Thermal Issues in Lithium-Ion Batteries," *Journal of the Electrochemical Society* 158 (2011): R1, https://doi.org/10.1149/1.3515880.

14. M. Asker, E. Alptekin, A. Tokuç, M. A. Ezan, and H. Ganjehsarabi, "The Effect of Phase Change Material Incorporated Building Wall on the CO_2 Mitigation: A Case Study of Izmir, Turkey," *International Journal of Global Warming* 19 (2019): 54, https://doi.org/10.1504/IJGW.2019.101772.

15. E. Revello, P. Dixit, K. Turunen, A. Santasalo-Aarnio, and A. H. Monteverde, "Assessment of Phase Change Materials for Thermal Energy Storage in Battery Systems for Heavy-Duty Vehicle Applications," *Energy Conversion and Management* 349 (2026): 120816, https://doi.org/10.1016/j.enconman.2025.120816.

16. E. Mandev, M. A. Ceviz, F. Afshari, and B. Muratçobanoğlu, "Evaluating PCM Heat Battery as a Range-Saving Solution for Electric Vehicle Cabin Heating," *Sustainable Energy Technologies and Assessments* 76 (2025): 104270, https://doi.org/10.1016/j.seta.2025.104270.

17. P. Xie, L. Jin, G. Qiao, C. Lin, C. Barreneche, and Y. Ding, "Thermal Energy Storage for Electric Vehicles at Low Temperatures: Concepts, Systems, Devices and Materials," *Renewable and Sustainable Energy Reviews* 160 (2022): 112263, https://doi.org/10.1016/j.rser.2022.112263.

18. T. Knote, B. Haufe, and L. Saroch, *E-Bus-Standard: Ansätze zur Standardisierung und Zielkosten für Elektrobusse* (Fraunhofer Institute for Transportation and Infrastructure Systems (IVI), 2017).

19. S. Kuitunen, "Thermal Storage Based Heating System for Full Electric City Buses," in 7th International Conference on Thermal Management for EV/HEV (2018), https://doi.org/10.13140/RG.2.2.24919.57766.

20. M. Sun, T. Liu, X. Wang, et al., "Roles of Thermal Energy Storage Technology for Carbon Neutrality," *Carbon Neutrality* 2 (2023) 12, https://doi.org/10.1007/s43979-023-00052-w.

21. S. Aykut Korkmaz, S. Ayten Çetinkaya, O. Yuksel, O. Konur, K. Emrah Erginer, and C. Ozgur Colpan, "Comparison of Various Metaheuristic Algorithms to Extract the Optimal PEMFC Modeling Parameters," *International Journal of Hydrogen Energy* 51 (2024): 1402–1420, https://doi.org/10.1016/j.ijhydene.2023.09.288.

22. Z. Abdin, C. J. Webb, and E. M. A. Gray, "PEM Fuel Cell Model and Simulation in Matlab–Simulink Based on Physical Parameters," *Energy* 116 (2016): 1131–1144, https://doi.org/10.1016/j.energy.2016.10.033.

23. J. C. Amphlett, R. M. Baumert, R. F. Mann, B. A. Peppley, P. R. Roberge, and T. J. Harris, "Performance Modeling of the Ballard Mark IV Solid Polymer Electrolyte Fuel Cell: II . Empirical Model Development," *Journal of the Electrochemical Society* 142 (1995): 9–15, https://doi.org/10.1149/1.2043959.

24. B. Yilmaz and C. O. Colpan, "Performance Analysis of a Small-Sized Hybrid Vehicle on a Real-World Inclined Route under WLTP, ARTEMIS, and NEDC Drive Cycles," *Fuel Cells* 26 (2026): e70073, https://doi.org/10.1002/fuce.70073.

25. Z. Zhao, T. Wang, B. Zhang, Y. Wang, C. Bao, and Z. Ji, "Analysis of an Integrated Thermal Management System With a Heat-Pump in a Fuel Cell Vehicle," *AIP Advances* 11 (2021): 065307, https://doi.org/10.1063/5.0056364.

26. S. Bashiri Mousavi and P. Ahmadi, "Enhancing the Performance of Hybrid Battery-Fuel Cell Electric Buses: Optimal Component Sizing, Thermal Systems Effect, and Power Source Durability," *Journal of Energy Storage* 149 (2026): 120104, https://doi.org/10.1016/j.est.2025.120104.

27. M. Asker, H. Ganjehsarabi, and M. Turhan Coban, "Numerical Investigation of Inward Solidification Inside Spherical Capsule by Using Temperature Transforming Method," *Ain Shams Engineering Journal* 9 (2018): 537–547, https://doi.org/10.1016/j.asej.2016.02.009.

28. T. LaClair, Z. Gao, O. Abdelaziz, M. Wang, E. Wolfe, and T. Craig, "Thermal Storage System for Electric Vehicle Cabin Heating - Component and System Analysis," SAE 2016 World Congress and Exhibition (2016), https://doi.org/10.4271/2016-01-0244.

29. A. M. Khudhair and M. M. Farid, "A Review on Energy Conservation in Building Applications With Thermal Storage by Latent Heat Using Phase Change Materials," *Energy Conversion and Management* 45 (2004): 263–275, https://doi.org/10.1016/S0196-8904(03)00131-6.

30. R. Sabbah, R. Kizilel, J. R. Selman, and S. Al-Hallaj, "Active (Air-Cooled) vs. Passive (Phase Change Material) Thermal Management of High Power Lithium-Ion Packs: Limitation of Temperature Rise and Uniformity of Temperature Distribution," *Journal of Power Sources* 182 (2008): 630–638, https://doi.org/10.1016/j.jpowsour.2008.03.082.

31. I. Dincer and M. A. Rosen, *Thermal Energy Storage: Systems and Applications*, 2nd ed. (Wiley, 2011).

32. RUBITHERM, *RT-Series Phase Change Materials: Product Data Sheet RT54* (RUBITHERM, 2026).